Multimodal image-guided interventions using oncological biomarkers

Stammes, M.A.

Chapter 4

Fluorescence- and multispectral optoacoustic imaging for an optimised detection of deeply located tumors in an orthotopic mouse model of pancreatic carcinoma

Joanna Napp*, Marieke A. Stammes*, Jing Claussen, Hendrica A.J.M. Prevoo, Cornelis F. M. Sier, Freek J. M. Hoeben, Marc S. Robillard, Alexander L. Vahrmeijer, Tim Devling, Alan B. Chan, Lioe-Fee de Geus-Oei, Frauke Alves.
*equal contribution

Adapted from: Fluorescence- and multispectral optoacoustic imaging for an optimised detection of deeply located tumors in an orthotopic mouse model of pancreatic carcinoma, Int J Cancer 2017 Dec 26. Doi:10.1002/ijc.31236

Abstract

Purpose

A crucial point for the management of pancreatic ductal adenocarcinoma (PDAC) is the decrease of R1 resections. Our aim was to evaluate the combination of multispectral optoacoustic tomography (MSOT) with fluorescence-guided surgery (FGS) for diagnosis and perioperative detection of tumor nodules and resection margins in a xenotransplant mouse model of human pancreatic cancer. As MSOT and FGS are novel technologies which can be used to improve visualisation of specifically labeled tissue.

Procedures

The peptide cRGD, conjugated with the near infrared fluorescent (NIRF) dye IRDye800CW and with a transcyclooctene (TCO) tag for future click chemistry (cRGD-800CW-TCO), was applied to PDAC bearing immunodeficient nude mice. 27 days after orthotopic transplantation of human AsPC-1 cells into the head of the pancreas, mice were injected with cRGD-800CW-TCO and imaged with fluorescence- and optoacoustic imaging devices before and 2h, 6h and 24h after injection, before they were sacrificed and dissected with the guidance of a FGS imaging system.

Results

Fluorescence imaging of cRGD-800CW-TCO allowed detection of the tumor area but without information about the depth, whereas MSOT allowed high resolution 3D identification of the tumor area, in particular of small tumor nodules. Highly sensitive delineation of tumor burden was achieved during FGS in all mice. Imaging of whole-mouse cryosections, histopathological analysis and NIRF microscopy confirmed the localization of cRGD-800CW-TCO within the tumor tissue.

Conclusion

In principle all imaging modalities applied here were able to detect PDAC *in vivo* using one NIRF probe. However, the combination of MSOT and FGS provided detailed spatial information of the signal, and achieved a complete overview of the distribution and localization of cRGD-800CW-TCO within the tumor before and during surgical intervention which could lead to a reduction in R1 resections in PDAC surgery.

Introduction

Pancreatic ductal adenocarcinoma (PDAC) has an extremely poor prognosis which is ascribed to the asymptomatic early phase of the disease and its aggressive tumor biology. The challenge in the management of operable pancreatic tumors is an achievement of R0 resections, i.e. complete removal of all tumor nodules. Unfortunately, 80% of pancreatic cancer surgeries are R1 resections, resulting in a further decreased overall survival[1,2].

Although surgeons still mostly rely on their visual perception and palpation, novel imaging methods such as fluorescence-guided surgery (FGS) are evolving to assist the differentiation of healthy and tumor tissue. FGS, typically based on near infrared (NIR) fluorescent probes visualises the desired structures in real time[3]. The application of planar NIR fluorescence imaging for non-invasive detection of tumors is restricted to approximately one cm deep structures[3,4]. Furthermore, the strong influence of tissue microenvironment and the light scattering hamper signal quantification[5,6]. Moreover, the detected fluorescence is projected onto the photographic image of the body surface in 2D and attribution to specific organs and structures within the body is not warranted. Nevertheless, planar fluorescence imaging is widely used in preclinical settings and increasingly applied in the clinic as it is non-invasive, easy-to-use, economic and possible in real-time.

Optoacoustic (also called photoacoustic) imaging is an emerging technology, which uses pulsed laser light to excite absorbing molecules. Those molecules undergo thermoelastic expansion leading to the release of acoustic waves[7,8]. With multispectral optoacoustic tomography (MSOT), tissue can be sequentially illuminated at different wavelengths and images can be processed using spectral unmixing algorithms in order to distinguish and quantify the contribution of different chromophores in tissue which can be spatially resolved and back-projected to reconstruct a three-dimensional (3D) image[9]. MSOT delivers anatomical and functional information simultaneously, with a high spatial resolution and up to 5 cm penetration depths, making it suitable for imaging deeper tissues and tumors within the body[10,11]. Nevertheless, the depth is dependent on the ultrasound frequency, with lower frequencies allowing for greater imaging depth but with a lower spatial resolution[12]. MSOT has been shown to address a number of clinically relevant aspects such as tissue oxygenation or tumor spreading and can potentially overcome a number of other shortcomings in current surgical practice[13-15].

Both optoacoustic and fluorescence imaging are relying on tumor specific probes[4,16]. Although there are numerous fluorescent dyes in every desired wavelength, currently, only very few of them are approved for the routine use in patients[17] IRDye800CW is one of the most promising new generation NIRF dyes, which can be detected by both, fluorescence and optoacoustic imaging and is currently widely tested in clinical trials[18]. Clinical evaluation is possible, as biocompatibility studies of 800CW did not show evidence of toxicity[19,20].

Here, we decided to use a cyclic arginine–glycine–aspartic acid (cRGD) peptide to target integrins, which are overexpressed in various cancer types and are playing a key role in the early phase of tumor angiogenesis and in tumor cell migration[21]. The cRGD peptide contains only one labeling site, for the 800CW dye, in contrast to other targeting molecules, like antibodies, which usually contain multiple labeling sites and can therefore vary in dye to protein ratios. Therefore quenching effects from dye–dye interactions caused by multiple labeling are avoided. In the clinic, several RGD constructs are already applied for tumor detection using PET or SPECT[22].

The combination of cRGD and IRDye800CW has already been tested in several preclinical studies, e.g. to specifically target integrins in a transgenic mouse model of glioblastoma or to provide high precision delineation of tumor tissue during fluorescence-guided glioblastoma resection[23]. In an orthotopic head and neck cancer model cRGD-800CW was efficiently combined with a unique handheld spectroscopic device for sensitive detection of integrin overexpression on infiltrating tumor cells for intraoperative visualization of not only invasive tumor margins but also metastatic lymph nodes[24]. In a subcutaneous PDAC model cRGD-800CW allowed for visualization of the tumor up to 24h post injection using fluorescence tumor imaging[25].

For future pre-targeting possibilities with a radiolabel to irradiate left over tissue a *trans*-cyclooctene (TCO) tag is already added. This system is based on the tumor-binding of a tagged molecule, cRGD-800CW, and the subsequent binding of a small fast-clearing radiolabeled molecule to cRGD-800CW. This will result in improved tumor to background ratios (TBRs) and local radionuclide therapy[26].

In this study we evaluated cRGD-800CW-TCO as a potential tool for FGS and more importantly as a tool to compare the diagnostic values of planar fluorescence imaging techniques with MSOT for *in vivo* preclinical imaging of deep seated tumors.

Materials & Methods

Probe preparation

The preparation of cRGD-800CW-TCO composed of *c[RGDyK]-IRDye800CW-(trans-cyclooctene)* is extensively described in the supplementary material section and is described in summary in **Figure 1**.

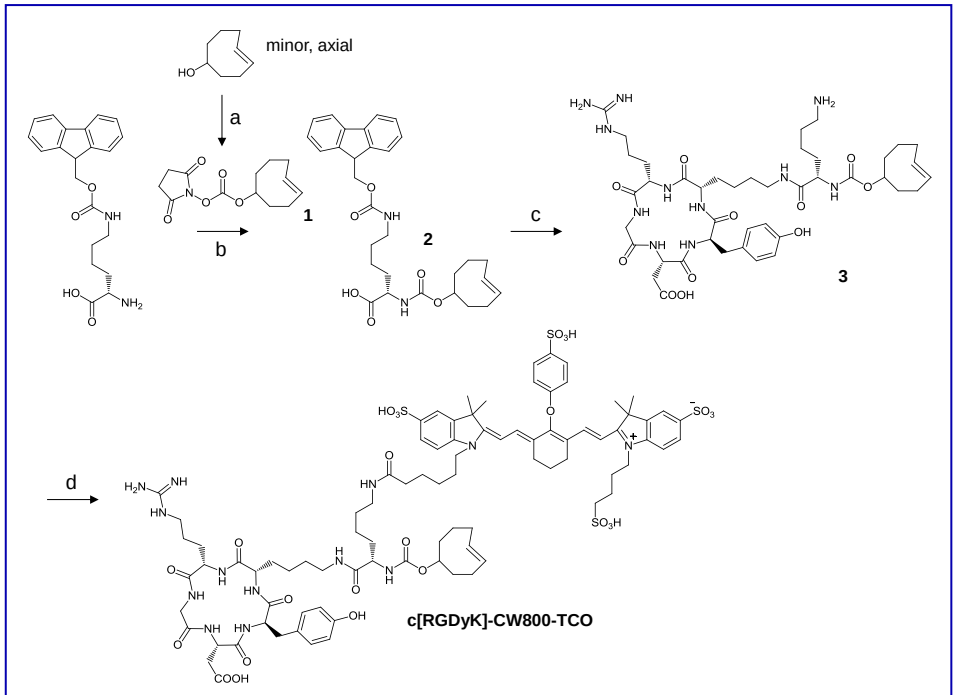

Figure 1. Synthesis of c[RGDyK]-IRdye800CW-TCO (cRGD-800CW-TCO)

(a) *N,N'-Disuccinimidylcarbonate, triethylamine, acetonitrile, r.t., 70 h, 58 %* ***(b) 1****, N,N-diisopropylethylamine, DMF / H_2O, r.t., 2 h, 62 %* ***(c)*** *i. 2,3,5,6-tetrafluorophenol, pyridinium-p-toluenesulfonate, N-(3-dimethylaminopropyl)-N'-ethylcarbodiimide hydrochloride, dichloromethane, r.t., 3 h, 83 %; ii. c[RGDyK]-NH_2, N,N-diisopropylethylamine, DMF, r.t., 1 h; iii. piperidine, DMF, 79 % over two steps* ***(d)*** *IRDye800CW NHS ester, N,N-diisopropylethylamine, DMF / DMSO, r.t., 1 h, 64 %.*

Cell line and culture conditions

The human PDAC cell line AsPC-1 was purchased from ATCC (Rockville, MD), cultivated as described before and used for all tumor models[27].

Animal studies

All animal experiments were performed in accordance with German animal ethics regulations, approved by the local ethics office of Lower Saxony (license no. 33.9–42502-04–13/1085). Experiments were performed on male athymic nude mice NMRI-*Foxn1*^{nu} (Charles River Laboratories), housed in ventilated cages and allowed food and water *ad libitum*.

For the subcutaneous (s.c.) transplantation 1 x 10^6 AsPC-1 cells were resuspended in 100 µl of PBS and transplanted into the left flank under brief isoflurane gas anesthesia (Abbvie, ~2%, 0.8 l/min). For the orthotopic transplantation 1 x 10^6 AsPC-1 cells were resuspended in 20 µl of PBS and implanted under xylazine (15 mg⁄ kg) ketamine (75 mg⁄ kg) anesthesia as described before[27]. Mice were sacrificed by isoflurane overdose and cervical dislocation.

Imaging

All *in vivo* analyses were preceded by native scans (0h). 27 days after transplantation, AsPC-1 tumor bearing mice received intravenously (i.v.) a single dose of cRGD-800CW-TCO (10 nmol in 100 µl of 0.9% NaCl) and were scanned under isoflurane gas anesthesia (2%, 0.8 l/min) with planar fluorescence imaging systems Optix MX2 (ART; timedomain system) and IVIS Spectrum (Perkin Elmer; epi-/trans-illumination system) as well as the small animal optoacoustic imaging system MSOT inVision 256-TF (iThera Medical GmbH) at 2h, 6h and 24h post injection (p.i.). Mice were sacrificed either 6h (n=3) or 24h (n=4) p.i. and one mouse per time-point was frozen (-20 °C) directly after sacrifice and used for whole body cryosectioning[28], the other for fluorescence-guided dissection (FGD) with the Artemis (Quest Diagnostics; epi-illumination) was performed to mimic FGS[29].

Spectrometer measurements

The probe was diluted in a solution of 10% BSA in saline with a final optical density of 0.17. The absorbance spectrum was measured in a 96-well plate between 680 nm and 900 nm at equidistant intervals of 10 nm using SpectraMax™ M2e (Molecular Devices). The probe spectrum was normalized to the maximum peak absorbance value.

Phantom measurement

The same diluted probe sample was then inserted inside 3 mm wide tubes at the center of a scattering cylindrical agar phantom (1.5% agar and 1% intralipid (Sigma); 2 cm diameter). MSOT acquisition was

performed in five imaging planes (~800 µm cross-section) with a 2 mm step size. Images were reconstructed and ROIs were drawn around the insertions to retrieve the mean signal intensities for each measured wavelength (680-900 nm).

***In vivo* NIRF imaging**

In Optix MX2, 730 nm excitation laser and 770 nm LP emission filter were applied for all scans. In vivo whole body scans and ex vivo imaging of organs were performed with 1.5 mm step size and 0.2 sec integration time per scan-point whereas the high-quality scans over the tumor area with 1.0 mm step size and 1.0 sec integration time. Optix 2.02.01 and OptiView 2.01.00 software (ART) were used to acquire and analyze the Optix MX2 data, respectively.

IVIS scans were performed with an excitation filter of 745 nm with 30 nm bandwidth, emission of 800 nm (range 780-840 nm), field of view (FOV) C for the whole-body scans and FOV B for the focused tumor area scans, medium binning. Living Image software 4.4 (Perkin Elmer) was used for IVIS Spectrum image acquisition and analysis.

Optoacoustic imaging & reconstruction

For optoacoustic imaging, the MSOT inVision 256-TF small animal imaging system (iThera Medical, Munich, Germany) was used[30]. Briefly, a tunable optical parametric oscillator (OPO) pumped by an Nd:YAG laser provides excitation pulses with a duration of 9 ns at wavelengths from 680 nm to 980 nm at a repetition rate of 10 Hz with a wavelength tuning speed of 10 ms and a peak pulse energy of 100 mJ at 730 nm. Ten arms of a fiber bundle provide even illumination of a ring-shaped light strip of approx. 8 mm width. For ultrasound detection, 256 toroidally focused ultrasound transducers with a center frequency of 5 MHz (60% bandwidth), organized in a concave array of 270° angular coverage and a radius of curvature of 4 cm, are used.

For scanning, isoflurane anesthetized mice were covered with ultrasound gel (Parker), gently and tightly wrapped in cling film and placed in a warm water container. Anesthesia was maintained throughout the procedure.

MSOT images were acquired at six different wavelengths: 715 nm, 730 nm, 760 nm, 775 nm, 850 nm and 900 nm. For each wavelength, 10 consecutive frames were recorded and averaged. Data was fluence-

corrected (μs = 10 cm-1, μa = 0.022 cm-1 at 800 nm) to compensate for spectral coloring. Image reconstruction with standard backprojection and spectral unmixing were done using ViewMSOT™ software. Multispectral processing was performed using linear regression on the probe spectrum measured in the phantom. Probe signals were pseudo-colored in jet and overlaid on the corresponding anatomical images (800 nm single wavelength) displayed in grey scale. Maximum intensity images were generated using the 3D ViewMSOT™ software tools. Any adjustment to brightness, color, or contrast has been made to the entire image and applied to all images.
For quantification of probe signals, ROI analysis was performed on single image sections of the spectrally unmixed probe signals with the ROI analysis tool of ViewMSOT

Fluorescence-guided dissection (FGD)
Quest Spectrum clinical system for in vivo FGS supported by Artemis Capture Suite 1.1.2 software (Quest Diagnostics) was used for the dissection guidance applying settings of both visible and NIR light. For the visible light of low-pass filter of <640 nm was used. The NIR light was excited with a wavelength of 785 nm, emission was done with a high-pass filter of >808 nm. In addition, reflected excitation light was blocked by a 750-800 nm filter. The raw data could be saved as individual snapshots or a real-time movie for data analysis. Representative movie frames were selected and FIJI software was used to produce color-coded images[31].
Excised organs were first imaged with both, the Optix MX2 and IVIS systems and afterwards fresh frozen and stored at -80°C.

Cryoslicing with fluorescence imaging
The samples were cut at equidistant intervals of 0.5 mm throughout the thoraco-abdominal level. For fluorescence imaging of the cryosections a Leica cryostat (CM 1950, Leica Microsystems, GmbH, Wetzlar, Germany) was retrofitted with a self-made fluorescence imaging system with excitation at 740 nm and emission captured with a 780 nm long pass filter. The exposure time was 2.5 seconds[28].

Tissue staining

Frozen tissues were sectioned at 2.5 µm slices slice thickness and fixed for 10 min with acetone. For anti-Integrin αv staining, slides were incubated for 1h with rabbit monoclonal anti-Integrin αv antibody (ab179475, Abcam) diluted 1:10.000 in 1% BSA in PBS followed by 30 min incubation with goat ant-rabbit Alexa Fluor 546 (1:400; Mol. Probes). For staining of αvβ3 integrins, mouse monoclonal anti-integrin αv/β3 antibody (sc-7312) was transferred to PBS using a Superdex 75 size-exclusion column (500 ml bed volume, GE Healthcare), brought to pH 8.5 before and directly conjugated with Alexa Fluor 488 for 2h slowly rocking in the dark. Slides were incubated for 1h with the labeled anti-integrin αv/β3 antibody diluted 1:200 in 1% BSA in PBS. Three washing steps with PBS, 5 min each, were performed after each incubation steps. Tissues were mounted with ProLong Gold Antifade Reagent (Thermo Fisher) with DAPI. Haematoxylin and Eosin (HE) staining was performed as described elsewhere[32].

Tissue imaging and fluorescence microscopy

Tissue imaging was performed on 10 µm tumor cryosections obtained from PDAC bearing mice that received 10 nmol cRGD-800CW-TCO, using the Odyssey flatbed scanner (Licor Biosciences) and analyzed with the respective software. Fluorescence microscopy was performed with an Axiovert 200 M inverted microscope (Carl Zeiss Microscopy GmbH) equipped with a NIR-sensitive ORCA-ER digital camera (Hamamatsu). 708 +/-37.5 nm excitation and 809 +/-40.5 nm emission filter was used for the detection of 800CW. A filter was used for the detection of Alexa-Fluor 546 fluorescence and 365 +/- 12.5 nm excitation and 445 +/-25 nm emission filter was used for the detection of DAPI.

Image generation and processing were performed with the software AxioVision Rel.4.6 software and FIJI[31], respectively.

Results

Spectral features of the cRGD-800CW-TCO-derived signals measured with MSOT *in vivo* in the subcutaneous tumor were compared to MSOT measurements of the same probe embedded in a phantom and to spectroscopic characteristics of the probe *in vitro*. As shown in **Figure 2A**, the *in vitro* cRGD-800CW-TCO spectrum was clearly red-shifted when

compared to MSOT scans *in vivo* and in the phantom. Based on these results, spectral unmixing was performed in all further *in vivo* experiments, using the absorption spectrum found with the MSOT phantom instead of using the spectrophotometer absorption spectrum.

The binding of cRGD-800CW-TCO and the specificity of the MSOT signals were first confirmed in mice bearing subcutaneous AsPC-1 tumors (n=3) 6h after i.v. probe injection in comparison to planar fluorescence imaging. In both planar optical imaging systems, Optix MX2 (**Figure 2B**) and IVIS (**Figure 2C**), strong probe-derived fluorescence signals were observed over the palpable tumors. Interestingly, NIR fluorescence signals detected with Optix MX2 were almost exclusively co-localized with the tumor region, whereas with the IVIS system additional relatively strong

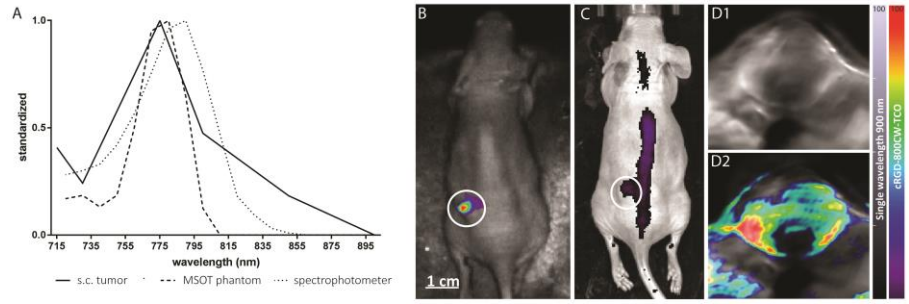

Figure 2. Characterisation of cRGD-800CW-TCO in a subcutaneous PDAC mouse model

(A) *Spectral analyses of in vitro, on phantom and in vivo data sets. The spectrum of cRGD-800CW-TCO measured with the spectrophotometer is clearly red-shifted in comparison to the spectra recorded in inVision 256-TF using i) cRGD-800CW-TCO dissolved in BSA and measured in a phantom and ii) the subcutaneous tumor.* ***(B)*** *Fluorescence intensity maps of the same tumor bearing mouse recorded 6h post injection (p.i.) of cRGD-800CW-TCO with Optix MX2 and* ***(C)*** *IVIS show clear accumulation of the probe in the subcutaneous (s.c.) AsPC-1 tumor (white circle). Fluorescence intensities are displayed in normalized counts.* ***(D)*** *InVision 256-TF scans show cRGD-800CW-TCO-derived optoacoustic signals in the transversal plane inside the subcutaneous tumor with a heterogeneous distribution pattern.* ***D1*** *= anatomical visualization,* ***D2*** *= distribution of cRGD-800CW-TCO.*

background fluorescence was observed, especially in the area surrounding the subcutaneous tumor and along the spine. Optoacoustic tomography revealed comparably strong probe-derived signals within the subcutaneous tumors but less background signals than planar fluorescence imaging, presumably coming from the remaining cRGD-800CW-TCO circulating in the bloodstream (**Figure 2D**). Notably, the transversal scans obtained with the MSOT system revealed

heterogeneous distribution of the probe within the tumor (**Figure 2D1**), suggesting areas with a different degree of cRGD-800CW-TCO accumulation (**Figure 2D2**).

MSOT allows *in vivo* 3D visualization of deeply located tumor nodules in the orthotopic PDAC mouse model

To validate the applicability of cRGD-800CW-TCO as a contrast agent for fluorescence- and optoacoustic imaging of deeply located tumors, an orthotopic mouse model of human PDAC was used in which AsPC-1 cells were transplanted into the head of the pancreas of nude mice. At the time of the imaging experiments - ~3.5 weeks after the transplantation - all mice had developed nodular primary tumors widely spread within the pancreas. The tumors generally showed invasion into the stomach and duodenum, and massive tumor spread to different distant sites and organs adjacent to the pancreas such as the liver, spleen or mesentery as well as growth of a tumor mass at the site of surgical incision (**Fig. 3A-D**). AsPC-1 tumor-bearing nude mice (n=7) were imaged with the OptixMX2, IVIS and MSOT before and 2h, 6h and 24h after i.v. injection of a single dose of cRGD-800CW-TCO (10nmol).

As shown in **Figure 3E**, OptixMX2 detected a strong fluorescence over the upper abdomen, where both, the primary PDAC tumor and the tumor mass at the site of surgical incision are located. The fluorescence intensity was highest at 2h p.i., decreased at 6h p.i., but was still clearly detectable at 24h p.i.. Heterogeneous background fluorescence was detectable at all scan time-points, which was presumably due to the presence of the circulating probe as well as a strong fluorescence signals from the excreted probe within the bladder. The highest tumor to background ratio (TBR) of 1.8±0.3 was measured with the OptixMX2 at 2h p.i. and decreased over time to 1.4±0.3 at 6h and 1.5±0.3 at 24h p.i.. A comparable fluorescence distribution pattern (**Figure 3F**) was obtained with the IVIS system with TBRs of 1.7±0.2 at 2h p.i., 2.0±0.2 at 6h p.i. and 2.2 ± 0.2 at 24h p.i..

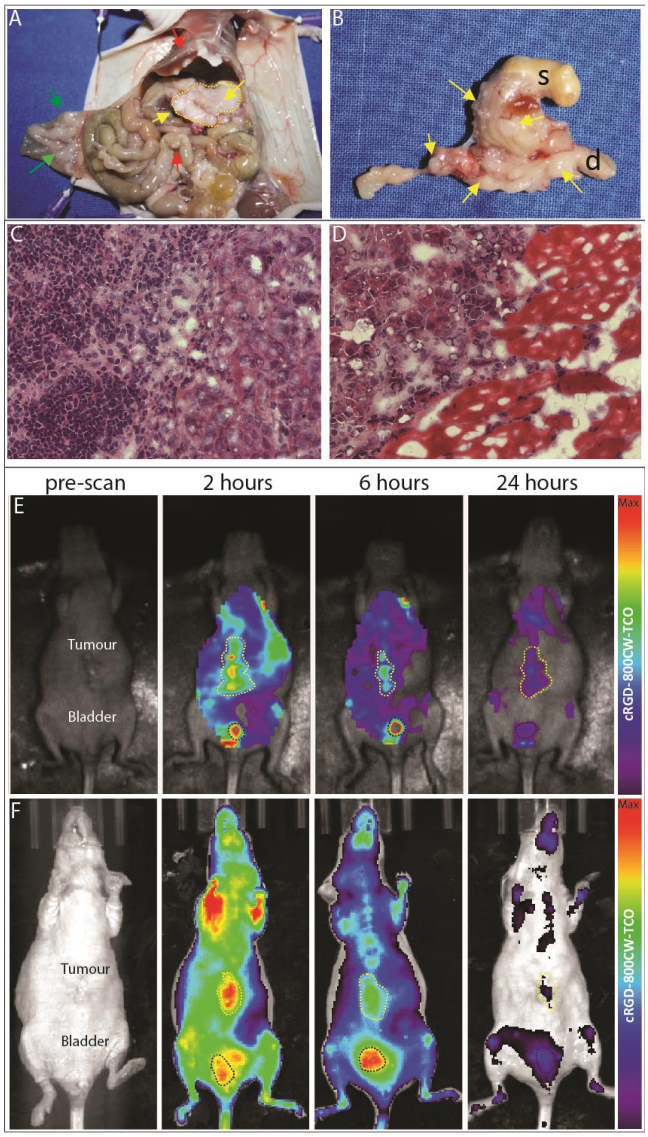

Figure 3. *In vivo* visualization of cRGD-800CW-TCO in an orthotopic PDAC mouse model

(A)-(D) *Representative morphological and histological appearance of an AsPC-1 tumour model.* ***(A)*** *Image of an AsPC-1 tumour bearing mouse taken during the dissection and showing the typical appearance of the primary tumour and extent of tumour spread within the abdomen (arrows: yellow = primary tumour, red = abdominal metastasis and green = tumour mass at the surgical scar).* ***(B)*** *Excised widely spread and nodular primary tumour (arrows) invading stomach (s) and duodenum (d).* ***(C)*** *HE staining of the primary tumour and* ***(D)*** *of the tumour mass at the site of surgical incision.* ***(E)*** *Representative ventral fluorescence whole body images of a mouse bearing an orthotopic AsPC-1 tumour, obtained before (pre-scan) and 2h, 6h and 24h p.i. of cRGD-800CW-TCO with Optix MX2 or* ***(F)*** *IVIS. Note the strong fluorescence signals from the excreted probe within the bladder. Fluorescence intensities are displayed in normalized counts.*

We observed that mice which developed a large tumor mass at the surgical scar at the abdominal wall also showed higher cRGD-800CW-TCO-derived fluorescence intensities (**Figure 4**). These findings suggest that the epifluorescence signals detected over the abdominal area are the sum of the fluorescence from the probe bound to the primary tumors and to the tumor mass grown at the surgical scar.

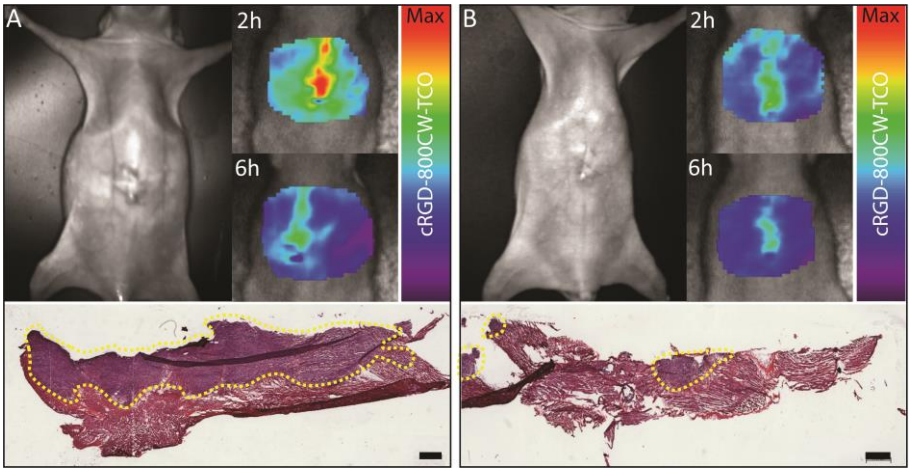

Figure 4. Detection of cRGD in relation to the tumour mass developed at the site of surgical incision.

Two representative mice showing (A) large and (B) small tumour mass at the laparotomy site are shown. Upper panels show photographic images (left) together with epifluorescence scans over the abdominal area (right) performed 2h and 6h post cRGD-800CW-TCO injection. Lower panels show HE histological staining of the corresponding area of the scar. Yellow dotted lines edge tumour areas. Scale bars: 1000 µm

Next, we used MSOT (**Figure 5**) to visualize the position of the primary tumor and tumor nodules in 3D, and to analyze the biodistribution and clearance of the probe over time (see Supplementary Material). **Figure 5A** shows representative MSOT transversal single slices through the mouse body at the level of the liver (1), the kidneys (2) and the bladder (3) and corresponding maximum intensity projections (MIPs) at 6h p.i. of the cRGD-800CW-TCO probe. The virtual positions of the slices are schematically depicted in **Figure 5B** in relation to the planar fluorescence image.

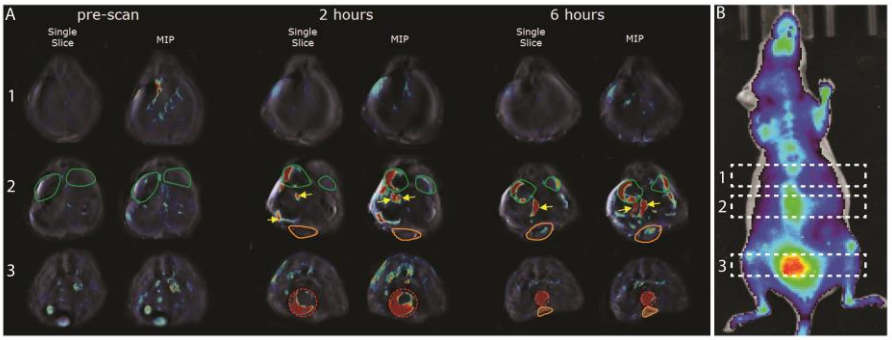

Figure 5. 3D *in vivo* visualization of PDAC by MSOT using cRGD-800CW-TCO

(A) *Representative MSOT scans of an orthotopic PDAC bearing mouse are shown as transversal spectrally unmixed single-slice images and maximum intensity projections (MIPs).* ***A1)*** *represents the liver level,* ***(A2)*** *the primary tumor level (orange solid line = scar tumor, yellow arrows = tumor nodules) and kidney level (green solid line), and* ***(A3)*** *the bladder level (red dotted line).* ***(B)*** *The corresponding location of the planes 1-3 of Figure 5A is schematically depicted on a whole body scan of the same tumor bearing mouse taken with the IVIS system.*

Using MSOT we could not only detect a clear accumulation of cRGD-800CW in the primary tumor but also in several deeply located tumor nodules (**Figure 5A**), which were clearly distinguishable from the primary tumor. Interestingly, we detected only very low background signals from the circulating probe, reflected in high TBRs of 29.5±0.9 at 2h, 33.5±0.9 at 6h, and TBRs of 49.3±2.8 at 24h p.i..

Furthermore, using MSOT, we could clearly confirm the renal excretion pathway of cRGD-800CW-TCO which is typical for small molecules: both, MSOT images (**Figure 5A**) and biodistribution results (see **Figure 6**), revealed a strong detection of probe-derived signals in the kidneys (plane 2; green) and in the bladder (plane 3; red dashed line), but not in the liver (plane 1).

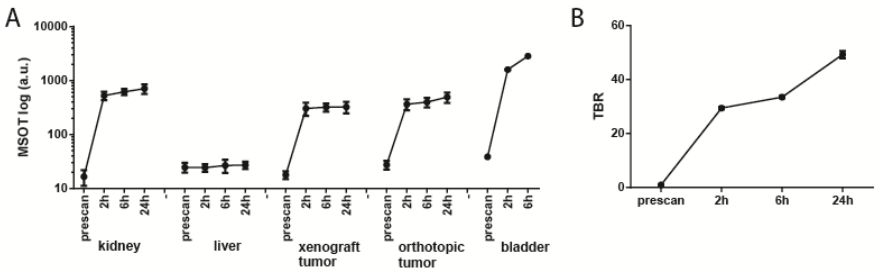

Figure 6. Analysis of *in vivo* biodistribution of cRGD-800CW with MSOT

(A) *shows signal intensities for cRGD-800CW in kidney, liver, xenograft tumor, orthotopic tumor and bladder before and at several timepoints after injection.* ***(B)*** *shows raise of TBR signal in single representative deep seated orthotopic tumors before and at several timepoints after injection. In mean, a ~50 fold raise was determined.*

cRGD-800CW-TCO enables FGD of PDAC

Finally, FGD was performed in the orthotopic PDAC model with the guidance of the clinical system Artemis (Quest Spectrum; epi-illumination), in order to assess the value of cRGD-800CW-TCO for the delineation of the margins between normal and PDAC tissue during surgery. At both, 6h (**Figure 7A**) and 24h (**Figure 7B**) after cRGD-800CW-TCO injection, strong fluorescence signals over the central abdomen were detected with the open field camera even through the skin (*frame 1*). Following median laparotomy and removing the skin, the fluorescence detectable through the peritoneum became more prominent (*frame 2*). Opening the peritoneum revealed that the fluorescence was mainly located over the primary tumor area (*frames 3-5*) as well as over the tumor mass at the site of surgical incision (data not shown). In addition, a strong fluorescence was detectable over the kidneys and bladder, especially at 6h p.i., which most likely corresponds to excreted cRGD-800CW-TCO. Lower fluorescence was also detectable over organs known to have a high integrin expression such as the intestine and the uterus. As shown in **Figure 7C** FGS allowed a clear delineation of the tumor margins. In addition, *ex vivo* imaging shows an increased signal at both, the tumor and scar thereby confirming the findings mentioned above and with MSOT. The real-time images taken before and directly

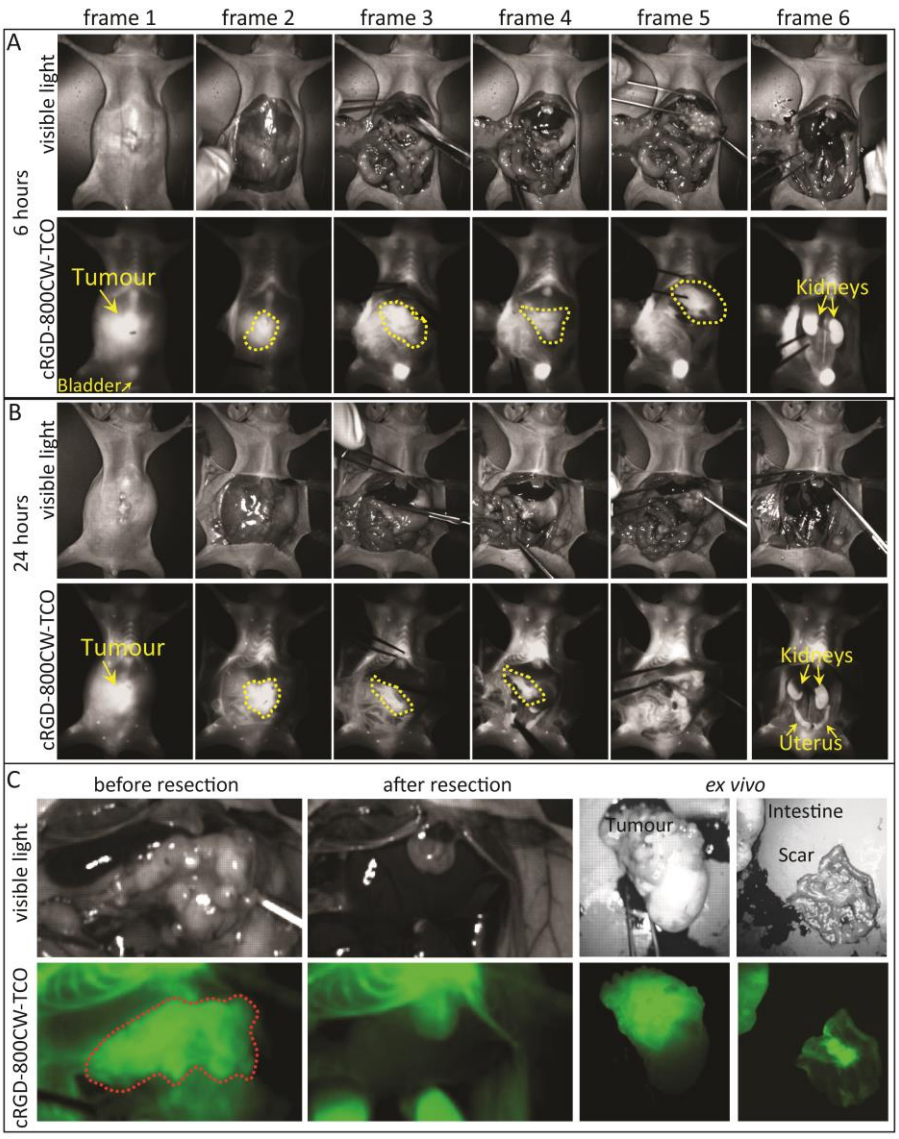

Figure 7. FGD of an orthotopic PDAC bearing mouse model

(A) *Representative images of an orthotopic PDAC bearing mouse at 6h and* ***(B)*** *24h p.i. of cRGD-800CW-TCO. Selected frames of representative movies (**frame 1-6**) recorded with the Artemis during different steps of the dissection are shown. At both time-points strong fluorescence intensities are detectable over the primary tumor area (yellow line). In addition, strong fluorescence is detectable over kidneys and bladder, especially at 6h p.i. and lower fluorescence over the intestine and uterus. Red arrows mark strong fluorescence over the tumor mass at the peritoneum.* ***(C)*** *Photographic and cRGD-800CW-TCO-derived fluorescence images recorded directly before (left) and after (middle) the resection of a primary tumour attached to the stomach and duodenum are shown. The margins of the primary tumour detected with FGS are delineated with red line. Note, that the fluorescence signals over the sternum and kidneys is still detectable after the resection. Panels on the right show the fluorescence signals over the resected primary tumour attached to the stomach and over the tumour mass at the surgical scar.*

after the resection of the pancreatic tumor tissue, together with stomach and duodenum, clearly confirmed that the resection bed is empty of the tumor-derived fluorescent signals upon removal of the cRGD labeled tissue, with only the background fluorescence remaining.

***Ex vivo* validation confirms accumulation of cRGD-800CW-TCO in an orthotopic PDAC mouse model**

To verify the accumulation of cRGD-800CW-TCO within the tumor and to validate the results from the *in vivo* fluorescence- and optoacoustic imaging, we performed various *ex vivo* analyses.

Two mice with orthotopic PDAC were sacrificed and frozen directly after their last scan (one at 6h p.i. and one at 24h p.i.) followed by cryosectioning of the entire body. Fluorescence distribution in the transversal cryosections with respect to the mouse anatomy was then compared to the signals obtained by spectral unmixing of MIPs of MSOT

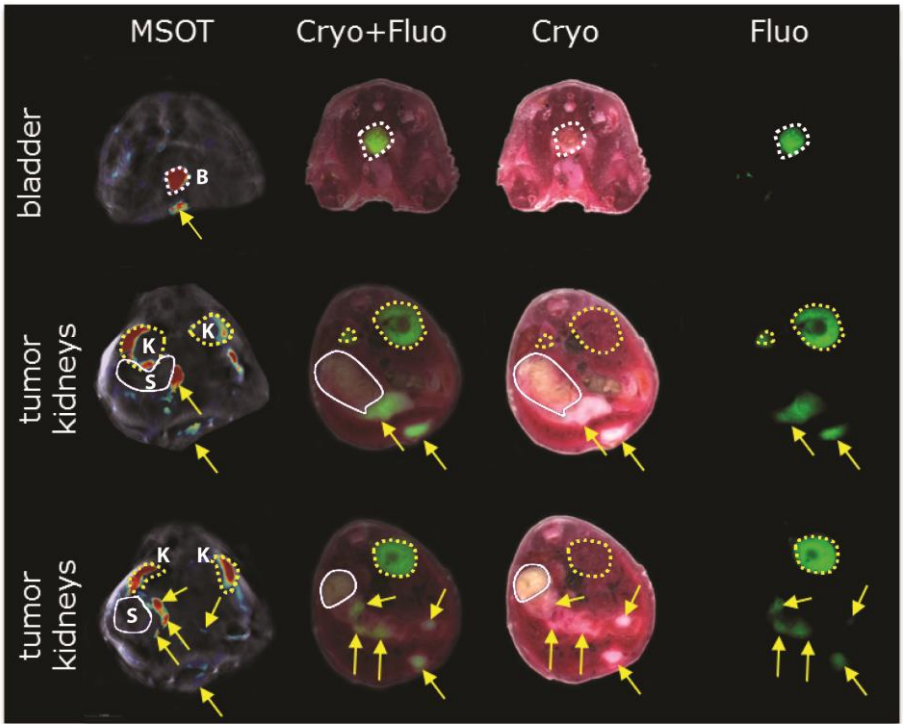

Figure 8. Histological analyses of cryosections in comparison to the fluorescence and optoacoustic images of whole mice

Representative transversal cryoslices (Cryo) of a PDAC bearing mouse sacrificed 6h p.i. of cRGD-800CW-TCO and the matching MSOT MIPs show almost identical distribution of the fluorescence (Fluo) and optoacoustic signals (MSOT) in the tumor pointed out by the yellow arrows. The yellow dotted lines outline the kidneys (K), the white lines the stomach (S) and the white dotted lines the bladder (B).

data. **Figure 8** shows representative transversal slices at the level of the bladder, the tumor and the kidneys for the PDAC mouse sacrificed at 6h p.i.. In both tested mice the *ex vivo* fluorescence measurements revealed a similar distribution pattern as the optoacoustic signals obtained *in vivo* with MSOT (**Figure 8,** yellow arrows).

Finally, excised samples of tumor tissue attached to the stomach and liver were cryosliced and analyzed with a flatbed fluorescence scanner before HE staining was performed. As shown in **Figure 9A-B**, strong cRGD-800CW-TCO fluorescence was predominantly found at the tumor margins allowing for a clear delineation of the tumor nodules (**Figure 9A**), with lower but still well detectable fluorescence within the central tumor mass. On a cellular level, co-staining of the tumor sections with antibodies targeting different integrins was
performed, in order to visualize the distribution of the *in vivo* injected probe, cRGD-800CW-TCO, in relation to the target. As shown in **Figure 9C**, the staining pattern of the anti-αvß3 integrin antibody (in blue) showed a highly similar pattern to that of the injected cRGD-800CW-TCO probe (in green). In contrast, anti-αv integrin antibody (in red) homogenously stained the tumor tissue, however without any correlation to the cRGD-800CW-TCO binding sites. The same staining pattern was observed on high resolution images (**Fig. 9D**).

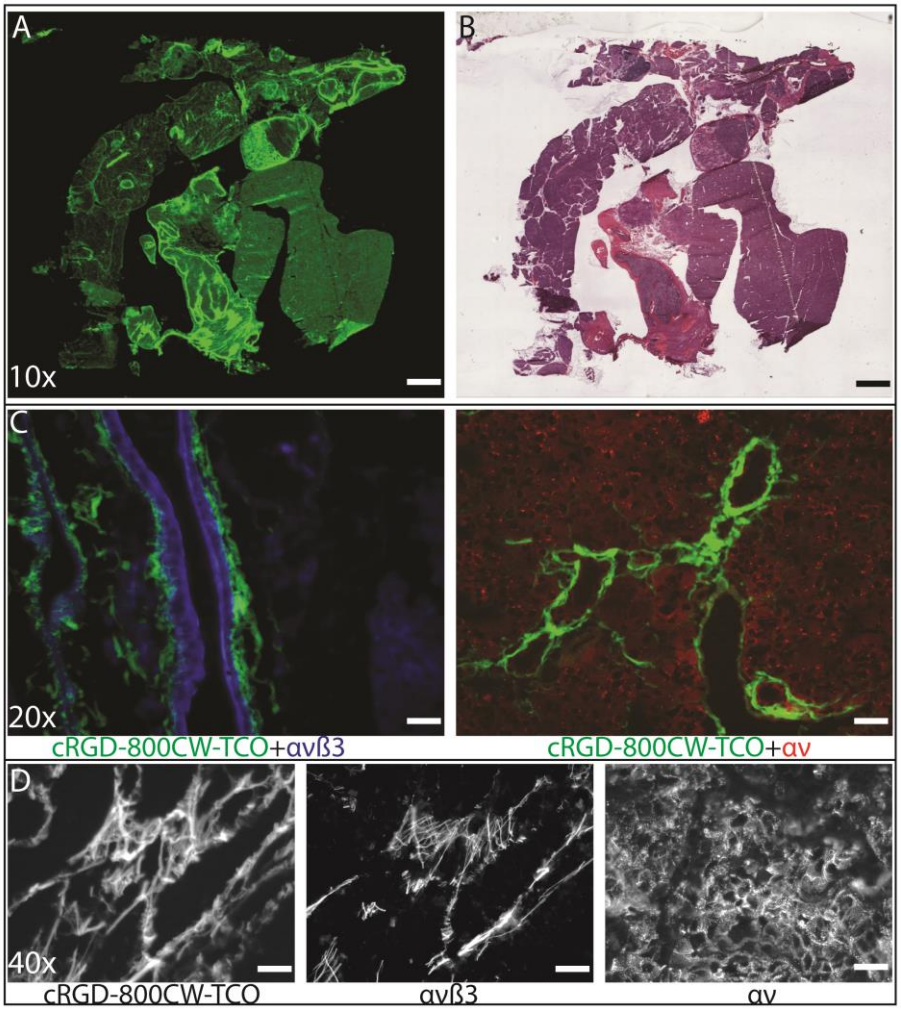

Figure 9. Histological analysis of PDAC samples obtained from FGD

(A) *Representative fluorescence scan of a cryoslice of the primary PDAC tumor attached to the stomach and liver and* ***(B)*** *corresponding HE staining of the same section demonstrating a strong accumulation of cRGD-800CW-TCO especially at tumor margins/invasion front (arrows).* ***(C,D)*** *Fluorescence microscopy of the tumor cryoslices shows co-localisation of cRGD-800CW-TCO only with anti-αvß3 integrin antibody but not with anti-αv integrin antibody staining. Scale bars in A and B: 2000 µm, C: 500 µm and D: 250 µm*

Discussion

To our knowledge, this is the first study showing the potential and feasibility of MSOT as a pre-operative imaging modality for the detection of deep-seated orthotopic pancreatic tumors in mice with an integrin targeting probe [33]. Using cRGD-800CW-TCO as a probe, we were able to distinguish the primary tumor and several small tumor nodules from healthy tissue non-invasively, with high specificity and by notably higher resolution than with planar fluorescence imaging. Finally, during FGD, which we used to mimic PDAC surgery, we not only confirmed the localisation of the tumor nodules detected by MSOT but could also clearly delineate tumor margins with high sensitivity.

In the first part of our study we analyzed the spectral characteristics of cRGD-800CW-TCO and found a clear red-shifted absorbance spectrum of the spectrometer compared to the *in vitro* and *in vivo* results by MSOT. This shift can be assigned to differences in relaxation times of probe molecules as they are excited with light pulses of different lengths[34]. *In vivo*, spectral coloring, the phenomenon by which light propagating through tissue undergoes wavelength specific fluence attenuation[35] or interactions with proteins might occur and cause wavelength shifts. Spectral unmixing of MSOT was performed after fluence correction using a linear regression algorithm and using the spectrum measured from the MSOT phantom in order to maximize the specificity of the unmixed results for cRGD-800CW-TCO. As this was closely correlated with the spectrum derived from the subcutaneous tumor we were confident that using the retrieved spectrum was an appropriate choice.

Using planar *in vivo* fluorescence imaging in cRGD-800CW-TCO injected orthotopic xenotransplants we were able to detect diffuse fluorescence signals over the upper abdomen, indicative of signal emanating from the primary tumor and/or from the tumor mass at the site of surgical incision. This however, did not allow for the precise localization of particular tumor nodules nor did it contain any information about the depth. In contrast, scanning the same mice with the MSOT resulted in high-resolution cross-sectional images from the abdominal area, which enabled the detection and localisation of the primary tumor and several deeply located small tumor nodules. In addition, by applying planar fluorescence imaging we obtained strong background signals, especially at early timepoints p.i. which were much lower in MSOT measurements, resulting in about 15-fold higher TBRs. This can be explained

by the fact that with planar fluorescence imaging all the fluorescence which reaches the object surface from different sources and depths after being subjected to absorbance and scattering, is collected and merged on the intensity maps. Consequently, the fluorescence of deeply located tumors appears less intense and more spread. Furthermore, the fluorescence from the circulating probe, especially in the surface-near areas can appear more intense, increasing the background signal and thereby decreasing the TBR. In this context, one advantage of MSOT over planar fluorescence imaging is the possibility to quantify signals in single slices (see SI) which leads to more reliable TBRs. Nevertheless, similar to fluorescence imaging, MSOT only allows a relative quantification of the signals. In both methods absolute quantification can only be achieved by a full correction for the absorption, scattering and anisotropy of the tissue, the technology to achieve this is still in its infancy[36,37]. Other methods such as gamma spectroscopy or mass spectrometry could be considered to be applied in future studies if absolute quantification of signals is needed.

Detection of pancreatic tumors with MSOT has previously been described [33]. Various probes have been used before, e.g. targeting Syndecan-1[33,38] or EGFR [39] and all of them allowed a clear and specific detection of probe derived optoacoustic signals over the primary tumors. However, in all these studies, pancreatic tumor cells were orthotopically transplanted into the tail of the pancreas which resulted in the development of only locally restricted tumors that grew on the left side of the abdomen next to the spleen and close to the body surface and were therefore relatively easy to localise. By contrast, in our study we transplanted PDAC cells into the head of the pancreas which resulted in the development of nodular primary tumors widely spread within the pancreas and located deep in the abdominal cavity, invading into the stomach and duodenum and accompanied with tumor mass growing at the site of surgical incision as well as multiple abdominal metastasis, as described by us and others [27,40]. This is a much more relevant model, as in humans about 65% of the pancreatic tumors arise in the head of the pancreas and only 15% in the body and tail [41]. Despite of this much more challenging model, we could clearly detect optoacoustic signals over the spread tumor nodules, showing that MSOT is highly suitable for the detection and discrimination of particularly deeply located and disseminated tumors.

Finally, by performing FGD of cRGD-800CW-TCO injected tumor-bearing mice we could confirm that the signals detected by the fluorescence camera during the surgery revealed similar patterns than those detected with MSOT before surgery. This shows that MSOT can provide a specific overview of the distribution and localization of the fluorescence signal at the tumor sites and therefore represents an ideal complement to the FGS. In contrast to planar fluorescence imaging - which has excellent sensitivity for superficial targets but becomes strongly limited by absorption and scattering of the incident and emitted light with increasing depth - MSOT is not susceptible to the scatter of emitted light. This makes MSOT more sensitive for imaging of deeply located tissue, as confirmed by the higher TBRs obtained with MSOT. Nevertheless, despite the clear advantages over planar fluorescence imaging such as high spatial resolution and increased penetration depth, MSOT still has its limitations. The work flow of MSOT is much slower than that of planar fluorescence imaging and includes i.e. multi-wavelength acquisition, reconstruction, spectral unmixing, and further 3D reconstruction, which can require additional post-processing and makes operation in real-time not always possible.

The development of MSOT instrumentation arose from the need for translational imaging. Although handheld optoacoustic devices are emerging, which can be handled similarly to classical ultrasound scan-heads, the current clinical translation of optoacoustic systems is still restricted to the detection of intrinsic absorbers such as haemoglobin, melanin or lipids or FDA approved unspecific contrast agents [13,42,43]. Several clinical trials using MSOT have already been performed [44], showing a powerful potential of the technique. However, without the availability of clinical available targeted probes, the full translation of optoacoustic imaging to the clinic is limited. Our study may support a progression in this direction.

Overall, we have demonstrated that cRGD-800CW-TCO can be used as a targeted probe to visualize orthotopic PDAC tumors with several optical imaging modalities. The TCO tag within the probe was designed for future therapeutic approaches based on the two step “click chemistry” principle, aiming future pre-targeting possibilities with a radiolabel to

irradiate left over tumor tissue. This would involve a two-step system with tumor-specific binding of cRGD-800CW-TCO as the first step and the subsequent binding of a small fast-clearing radiolabeled molecule to the TCO tag as the second step of the treatment. Click chemistry via TCO tag has already been shown to improve tumor specificity [26].

Nevertheless, in addition to the signals at the disseminated primary pancreatic tumors, we detected both, fluorescence- and optoacoustic signals at the abdominal wall. We ascribed these signals to the tumor mass developed at the scar of the laparotomy site, as the fluorescence intensity was in accordance with the size of the tumor mass present at the scar. Furthermore, we detected relatively high background signals from the circulating probe, as well as relatively high fluorescence from healthy tissue with a high cellular turnover such as intestine or uterus. This is not very surprising, as integrins in general orchestrate cell-cell and cell-extracellular matrix adhesive interactions from embryonic development to mature tissue function. In addition, the αvβ3 integrin, which is the major target for cRGD, is connected with angiogenesis, wound healing and cell migration [45]. We thus cannot exclude that some tissue remodelling processes involving integrins still take place at the scar tissue, which could be a source of part of the cRGD-derived signals over the upper abdomen. Taken together, this indicates that the RGD-targeting probe, although sufficient for the perioperative detection of tumor nodules, is not ideal for the improvement of the specificity of therapeutic approaches. Therefore, for clinical use, the choice of the target-ligand combination should be further optimised.

Altogether we showed, that MSOT has the unique ability to give an *in vivo* whole-body 3D overview of the distribution of the probe and its clinical pre-surgery application might provide surgeons with information about the tumor distribution and its interactions with the microenvironment and surrounding organs and structures.

Acknowledgements

We want to acknowledge Thomas C.P. Sardella for the great support during the MSOT recordings, Hannah Puchala, Bärbel Heidrich, Yuedan Li, Katja Bierau, Peter Küppen and Keely Pierzchalski for the help and technical assistance during the experiments, Henk Janssen for the technical assistance during the chemical construction of the probe. We thank Andrea Markus for critical proofreading of the manuscript.

Funding: this work was supported by a European Union project grant from H2020, H2020-MSCA-RISE grant number 644373—PRISAR.

References

1. Gillen S, Schuster T, Meyer Zum Buschenfelde C, Friess H, Kleeff J. Preoperative/neoadjuvant therapy in pancreatic cancer: a systematic review and meta-analysis of response and resection percentages. *PLoS Med.* 2010;7(4):e1000267.
2. Handgraaf HJ, Boonstra MC, Van Erkel AR, et al. Current and future intraoperative imaging strategies to increase radical resection rates in pancreatic cancer surgery. *Biomed Res Int.* 2014;2014:890230.
3. Vahrmeijer AL, Hutteman M, van der Vorst JR, van de Velde CJ, Frangioni JV. Image-guided cancer surgery using near-infrared fluorescence. *Nat Rev Clin Oncol.* 2013;10(9):507-518.
4. de Boer E, Harlaar NJ, Taruttis A, et al. Optical innovations in surgery. *Br J Surg.* 2015;102(2):e56-72.
5. Liu Y, Tseng YC, Huang L. Biodistribution studies of nanoparticles using fluorescence imaging: a qualitative or quantitative method? *Pharm Res.* 2012;29(12):3273-3277.
6. Hawe A, Sutter M, Jiskoot W. Extrinsic fluorescent dyes as tools for protein characterization. *Pharm Res.* 2008;25(7):1487-1499.
7. Mehrmohammadi M, Yoon SJ, Yeager D, Emelianov SY. Photoacoustic Imaging for Cancer Detection and Staging. *Curr Mol Imaging.* 2013;2(1):89-105.
8. Bowen T. Radiation-Induced Thermoacoustic Soft-Tissue Imaging. *Ieee T Son Ultrason.* 1982;29(3):187-187.
9. Taruttis A, Ntziachristos V. Advances in real-time multispectral optoacoustic imaging and its applications. *Nat Photon.* 2015;9(4):219-227.
10. Luke GP, Yeager D, Emelianov SY. Biomedical applications of photoacoustic imaging with exogenous contrast agents. *Ann Biomed Eng.* 2012;40(2):422-437.
11. Kim C, Erpelding TN, Jankovic L, Pashley MD, Wang LV. Deeply penetrating in vivo photoacoustic imaging using a clinical ultrasound array system. *Biomed Opt Express.* 2010;1(1):278-284.
12. Yao J, Wang LV. Photoacoustic Microscopy. *Laser Photon Rev.* 2013;7(5).
13. Knieling F, Neufert C, Hartmann A, et al. Multispectral Optoacoustic Tomography for Assessment of Crohn's Disease Activity. *N Engl J Med.* 2017;376(13):1292-1294.
14. Stoffels I, Morscher S, Helfrich I, et al. Metastatic status of sentinel lymph nodes in melanoma determined noninvasively with multispectral optoacoustic imaging. *Science translational medicine.* 2015;7(317):317ra199.
15. Taruttis A, Timmermans AC, Wouters PC, Kacprowicz M, van Dam GM, Ntziachristos V. Optoacoustic Imaging of Human Vasculature: Feasibility by Using a Handheld Probe. *Radiology.* 2016;281(1):256-263.
16. Cantisani V, Grazhdani H, Fioravanti C, et al. Liver metastases: Contrast-enhanced ultrasound compared with computed tomography and magnetic resonance. *World J Gastroenterol.* 2014;20(29):9998-10007.
17. Nguyen QT, Tsien RY. Fluorescence-guided surgery with live molecular navigation--a new cutting edge. *Nat Rev Cancer.* 2013;13(9):653-662.
18. Mercep E, Burton NC, Claussen J, Razansky D. Whole-body live mouse imaging by hybrid reflection-mode ultrasound and optoacoustic tomography. *Optics letters.* 2015;40(20):4643-4646.

19. Heuveling DA, Visser GW, de Groot M, et al. Nanocolloidal albumin-IRDye 800CW: a near-infrared fluorescent tracer with optimal retention in the sentinel lymph node. *Eur J Nucl Med Mol Imaging.* 2012;39(7):1161-1168.
20. Marshall MV, Draney D, Sevick-Muraca EM, Olive DM. Single-dose intravenous toxicity study of IRDye 800CW in Sprague-Dawley rats. *Mol Imaging Biol.* 2010;12(6):583-594.
21. Verbeek FP, van der Vorst JR, Tummers QR, et al. Near-infrared fluorescence imaging of both colorectal cancer and ureters using a low-dose integrin targeted probe. *Annals of surgical oncology.* 2014;21 Suppl 4:S528-537.
22. Chen H, Niu G, Wu H, Chen X. Clinical Application of Radiolabeled RGD Peptides for PET Imaging of Integrin alphavbeta3. *Theranostics.* 2016;6(1):78-92.
23. Huang R, Vider J, Kovar JL, et al. Integrin alphavbeta3-targeted IRDye 800CW near-infrared imaging of glioblastoma. *Clinical cancer research : an official journal of the American Association for Cancer Research.* 2012;18(20):5731-5740.
24. Yoon Y, Mohs AM, Mancini MC, Nie S, Shim H. Combination of an Integrin-Targeting NIR Tracer and an Ultrasensitive Spectroscopic Device for Intraoperative Detection of Head and Neck Tumor Margins and Metastatic Lymph Nodes. *Tomography.* 2016;2(3):215-222.
25. Liu L, Lin G, Yin F, Law WC, Yong KT. Near-infrared fluorescent peptide probes for imaging of tumor in vivo and their biotoxicity evaluation. *J Biomed Mater Res A.* 2016;104(4):910-916.
26. Rossin R, van Duijnhoven SM, Lappchen T, van den Bosch SM, Robillard MS. Trans-cyclooctene tag with improved properties for tumor pretargeting with the diels-alder reaction. *Molecular pharmaceutics.* 2014;11(9):3090-3096.
27. Saccomano M, Dullin C, Alves F, Napp J. Preclinical evaluation of near-infrared (NIR) fluorescently labeled cetuximab as a potential tool for fluorescence-guided surgery. *Int J Cancer.* 2016;139(10):2277-2289.
28. Sarantopoulos A, Themelis G, Ntziachristos V. Imaging the bio-distribution of fluorescent probes using multispectral epi-illumination cryoslicing imaging. *Molecular imaging and biology : MIB : the official publication of the Academy of Molecular Imaging.* 2011;13(5):874-885.
29. van Driel PB, van de Giessen M, Boonstra MC, et al. Characterization and evaluation of the artemis camera for fluorescence-guided cancer surgery. *Molecular imaging and biology : MIB : the official publication of the Academy of Molecular Imaging.* 2015;17(3):413-423.
30. Morscher S, Driessen WH, Claussen J, Burton NC. Semi-quantitative Multispectral Optoacoustic Tomography (MSOT) for volumetric PK imaging of gastric emptying. *Photoacoustics.* 2014;2(3):103-110.
31. Schindelin J, Arganda-Carreras I, Frise E, et al. Fiji: an open-source platform for biological-image analysis. *Nat Methods.* 2012;9(7):676-682.
32. Alves F, Contag S, Missbach M, et al. An orthotopic model of ductal adenocarcinoma of the pancreas in severe combined immunodeficient mice representing all steps of the metastatic cascade. *Pancreas.* 2001;23(3):227-235.
33. Yin W, Kimbrough CW, Gomez-Gutierrez JG, et al. Tumor specific liposomes improve detection of pancreatic adenocarcinoma in vivo using optoacoustic tomography. *J Nanobiotechnology.* 2015;13:90.

34. Laufer J, Jathoul A, Pule M, Beard P. In vitro characterization of genetically expressed absorbing proteins using photoacoustic spectroscopy. *Biomed Opt Express.* 2013;4(11):2477-2490.
35. Cox B, Laufer JG, Arridge SR, Beard PC. Quantitative spectroscopic photoacoustic imaging: a review. *J Biomed Opt.* 2012;17(6):061202.
36. Tzoumas S, Nunes A, Olefir I, et al. Eigenspectra optoacoustic tomography achieves quantitative blood oxygenation imaging deep in tissues. *Nat Commun.* 2016;7:12121.
37. Brochu FM, Brunker J, Joseph J, Tomaszewski MR, Morscher S, Bohndiek SE. Towards Quantitative Evaluation of Tissue Absorption Coefficients Using Light Fluence Correction in Optoacoustic Tomography. *IEEE Trans Med Imaging.* 2017;36(1):322-331.
38. Kimbrough CW, Hudson S, Khanal A, Egger ME, McNally LR. Orthotopic pancreatic tumors detected by optoacoustic tomography using Syndecan-1. *Journal of Surgical Research.* 2015;193(1):246-254.
39. Hudson SV, Huang JS, Yin WY, et al. Targeted Noninvasive Imaging of EGFR-Expressing Orthotopic Pancreatic Cancer Using Multispectral Optoacoustic Tomography. *Cancer Research.* 2014;74(21):6271-6279.
40. Napp J, Dullin C, Muller F, et al. Time-domain in vivo near infrared fluorescence imaging for evaluation of matriptase as a potential target for the development of novel, inhibitor-based tumor therapies. *International Journal of Cancer.* 2010;127(8):1958-1974.
41. Artinyan A, Soriano PA, Prendergast C, Low T, Ellenhorn JDI, Kim J. The anatomic location of pancreatic cancer is a prognostic factor for survival. *Hpb.* 2008;10(5):371-376.
42. McNally LR, Mezera M, Morgan DE, et al. Current and Emerging Clinical Applications of Multispectral Optoacoustic Tomography (MSOT) in Oncology. *Clinical cancer research : an official journal of the American Association for Cancer Research.* 2016;22(14):3432-3439.
43. Valluru KS, Willmann JK. Clinical photoacoustic imaging of cancer. *Ultrasonography.* 2016;35(4):267-280.
44. Whitley MJ, Weissleder R, Kirsch DG. Tailoring Adjuvant Radiation Therapy by Intraoperative Imaging to Detect Residual Cancer. *Semin Radiat Oncol.* 2015;25(4):313-321.
45. Zhao ZQ, Yang Y, Fang W, Liu S. Comparison of biological properties of Tc-99m-labeled cyclic RGD Peptide trimer and dimer useful as SPECT radiotracers for tumor imaging. *Nucl Med Biol.* 2016;43(11):661-669.